Magnetic correlation states in cosputtered granular $Ag_{100-x}Fe_x$ films

Paolo Allia,[1] Marco Coisson,[2] Federico Spizzo,[3] Paola Tiberto,[2] and Franco Vinai[2]
[1]*Dipartimento di Fisica, Politecnico di Torino and INFM, Research Unit Torino Politecnico, Corso Duca degli Abruzzi 24, I-10129 Torino, Italy*
[2]*Istituto Elettrotecnico Nazionale Galileo Ferraris and INFM, Research Unit Torino Politecnico, Strada delle Cacce 91, I-10135 Torino, Italy*
[3]*Dipartimento di Fisica, Universita di Ferrara and INFM, Research Unit Ferrara, Via Paradiso 12, I-44100 Ferrara, Italy*
(Received 17 May 2005; revised manuscript received 6 December 2005; published 6 February 2006)

Measurements of isothermal magnetization, initial and high-field static susceptibility, and magnetoresistance have been performed at various temperatures on five $Ag_{100-x}Fe_x$ granular films of variable Fe content ($10 \leqslant x \leqslant 30$) obtained by cosputtering. Magnetoresistance and magnetization data have been systematically combined to determine the magnetic correlation volume in each sample and its evolution with temperature and magnetic field. A coherent picture of the whole set of $Ag_{100-x}Fe_x$ films has been obtained. On increasing x, these alloys exhibit a magnetic behavior of increasing complexity, from the interacting superparamagnetic phase with weakly interacting magnetic moments and small correlation volumes to frustrated ferromagnetism with strong magnetic interactions, loss of physical identity of Fe particles, and extended correlation volumes. The degree of alignment of individual magnetic moments within a correlation volume and the stability of correlation volumes themselves against an external magnetic field are discussed in some detail.

DOI: 10.1103/PhysRevB.73.054409 PACS number(s): 75.75.+a, 73.63.−b, 72.25.Ba, 73.50.−h

I. INTRODUCTION

Nanogranular composite materials formed by combining magnetic and nonmagnetic elements exhibit exciting physical properties. These materials are of interest in data-storage technology (e.g., hard disk drives) as well as for fundamental studies concerning new phenomena induced by the nanostructure.[1] Tailor-made magnetic anisotropies, magnetic moment enhancement, superparamagnetic and ferromagnetic behavior in dependence of particle size and temperature, and magnetic exchange coupling are examples of important physical aspects that have placed this class of materials at the frontiers of research.[2,3] The reduced particle size, combined with specific nanostructures, provides granular materials with a rich variety of interesting physical properties, which can be subsequently used in the development of new types of devices, particularly in the area of magnetic recording.

Among these materials, a substantial role is played by granular magnetic systems consisting of nanometer-sized particles of a ferromagnetic metal (typically Fe or Co) embedded in a nonmagnetic metallic matrix (such as Ag, Au, Cu). Interest in these materials stems from the discovery of giant magnetoresistance (GMR) more than a decade ago,[4,5] a real breakthrough in pure and applied research on magnetotransport properties.

The GMR effect was first discovered in magnetic multilayers.[6,7] A GMR similar to the one found in multilayers was soon observed in granular systems also; this stimulated the study of transport properties in magnetically heterogeneous media, raising interest in the prospective applications of granular systems, which are very easy to produce by means of a number of off-equilibrium techniques (i.e., chemical vapor deposition, magnetron sputtering).[4,8,9] Moreover, it is observed that both magnetic properties and magnetoresistance strongly depend on specific aspects of the nanostructure, such as particle size distribution, mean interparticle distance, particle shape, roughness of the magnetic/nonmagnetic interfaces, and concentration of magnetic solute atoms.[4,5,10–12] Some of these properties can be suitably controlled by means of specific thermal treatments.[4,5]

Generally speaking, the GMR has been interpreted in terms of spin-dependent scattering of conduction electrons, occurring mainly at the magnetic/nonmagnetic interfaces or, more generally, at the edges of regions of magnetic coherence.[13,14] The $Cu_{100-x}Co_x$ system, obtained either by rapid solidification or sputtering, has emerged over the last decade as one of the most investigated materials,[4,5,9,15] because it displays a significant GMR effect. Recently, however, CoAg films have been shown to exhibit notable GMR values, particularly after annealing; the maximum GMR value (normalized to the R_∞ value) becomes as high as 40% in the annealed $Ag_{71}Co_{29}$ system, presumably owing to quenching of interparticle interactions.[12] In the case of $Cu_{100-x}Co_x$, the magnitude of the GMR effect is strictly related to both microstructural features and intergranular magnetic interactions.[16,17] As a consequence, the shape and size of the particles, together with crystal nucleation and growth, turned out to be crucial parameters for a fine-tuning of magnetotransport properties. However, a complete understanding of the relationship among microstructural properties and GMR has been hindered by the fact that conventional methods of structural analysis are hardly applicable to $Cu_{100-x}Co_x$ alloys, owing to low x-ray contrast between Co and Cu as well as to high lattice coherency and small lattice mismatch. This can be overcome by choosing other granular systems, such as cosputtered $Ag_{100-x}Fe_x$ films with variable Fe concentration. This composition deserves attention because of its high magnetoresistance[10] associated with good tunability of the relative concentration between ferromagnetic metal and metallic matrix. The deposition process has been observed to play an important role in structure evolution and thus affects the GMR. Moreover, the GMR is found to be very sensitive

to the Fe volume fraction, becoming smaller in both the Fe-poor and Fe-rich regions of the system.[10,18,19]

Even when x-ray diffraction can be properly exploited to relate the magnetoresistance to structural features (particle size distribution, different structural, and/or magnetic phases), a complete understanding of the magnetic properties of granular systems such as $Ag_{100-x}Fe_x$ is hindered by their complexity (i.e., interparticle magnetic interactions and local magnetic anisotropies of whatever origin). In fact, it is extremely difficult to properly understand which factor plays a dominant role in the magnetic behavior of granular systems, although this knowledge would contribute to optimize their fundamental properties for prospective technological applications. As a consequence, the role of interparticle interactions on the magnetic and magnetotransport properties of nanogranular systems is still debated.

Recently, a model combining the analysis of experimental magnetization and magnetoresistance data has been exploited to study the correlation among magnetic scatterers and its field and temperature dependence in various systems, such as magnetic granular ribbons or films and frustrated magnets with ultrashort ferromagnetic exchange length.[17] The model provides a figure of the magnetic correlation length, representing a characteristic maximum scale over which a sudden change in the orientation of any localized magnetic moment brings about a rearrangement of another localized moment.

In this work, the model is systematically exploited to investigate the different states of magnetic correlation emerging in the $Ag_{100-x}Fe_x$ system by effect of varying the concentration of the ferromagnetic metal.

II. EXPERIMENT

$Ag_{100-x}Fe_x$ granular films, where x represents the relative Fe volume concentration, were deposited on Si (100) substrates by the dc-magnetron cosputtering technique in Ar atmosphere. The background pressure in the experimental chamber was equal to 8×10^{-8} Torr; during deposition, the Ar sputtering pressure was kept at 10 mTorr. Two high-purity targets were used; different values of x were obtained by fixing the Fe sputtering rate and changing that of Ag. The total thickness of the films was determined with a quartz microbalance and found to be 250 nm. The substrate was kept at room temperature during deposition. Wide-angle x-ray diffraction and Mössbauer spectroscopy were exploited to get information on the intermiscibility of metals and on the environment of Fe atoms.[20]

Samples with $x=10,14,20,26,30$ were investigated through magnetic and magnetoresistance measurements. Magnetization loops were obtained at different temperatures in the 4–300 K range under a maximum applied field of 50 kOe using a Quantum Design superconducting quantum interference device (SQUID) magnetometer ($x\leqslant20$) and an Oxford Instruments MagLab 2000 system with extraction magnetometer ($x>20$). Initial and high-field susceptibilities were measured from the field derivatives of the measured curves. Magnetoresistance measurements were performed between 4 K and 270 K by means of the four-contact method with soldered electrical contacts, under an in-plane applied field provided by the MagLab system (maximum value: 70 kOe). The magnetoresistance $MR(H,T)$ is defined as $[R(H)-R(0)]/R(0)\times100$. The maximum magnetoresistance MR_{max} is defined as $[R(70\ \text{kOe})-R(0)]/R(0)\times100$. In the experimental configuration, the magnetoresistance was measured with the current flowing in the plane of the film, parallel to the magnetic field (longitudinal configuration).

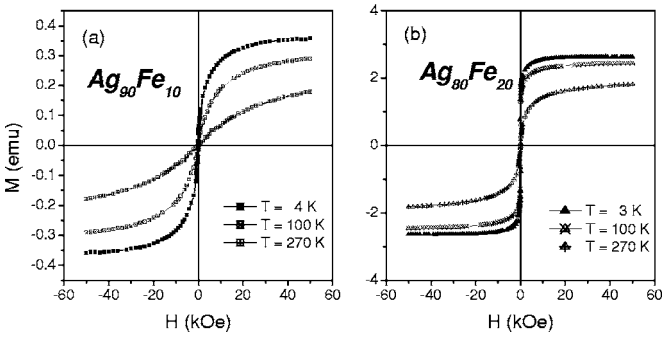

FIG. 1. Isothermal magnetization curves of $Ag_{90}Fe_{10}$ and $Ag_{80}Fe_{20}$-cosputtered films at selected temperatures.

The signals detected by both magnetometers are proportional to the magnetic response of the whole samples, inclusive of the contribution from the diamagnetic substrate. The diamagnetic contribution was routinely subtracted after recording the response of a blank sample (i.e., substrate only) at all temperatures. The magnetometers provide the magnetic moment of each film; reliable magnetization values (magnetic moment per unit volume or per unit mass) cannot be obtained owing to the uncertain determination of both film volume and mass. On the contrary, the saturation magnetization is determined with a much higher degree of confidence through extrapolation of the high-field magnetization curves. As a consequence, most of the ensuing discussion will be based upon *reduced* magnetization and susceptibility values. The reduced magnetic susceptibility $\tilde{\chi}=\chi/M_S$ will be expressed in Oe^{-1}. For all films except $Ag_{86}Fe_{14}$, seven temperatures between 4 and 270 K were routinely examined. In the case of $Ag_{86}Fe_{14}$, only three temperatures were investigated.

III. RESULTS: MAGNETIZATION MEASUREMENTS

Isothermal magnetization curves of films with $x\leqslant20$ exhibit superparamagnetic features, such as the absence of measurable hysteresis at high temperatures and a slowly saturating high-field behavior. Typical examples are provided in Fig. 1 for $x=10$ and 20 at selected temperatures. Similar data were obtained for $x=14$. A more accurate inspection reveals a hardly detectable hysteresis loop at $T=4$ K (coercivity $H_C\approx400$ Oe, almost independent of x). In the following, this small hysteresis (which decreases with increasing T and completely disappears above the blocking temperature of each composition) will be neglected.

The measured data indicate that films with $x\leqslant20$ are in the interacting superparamagnetic (ISP) phase[21] in most of the investigated temperature range. Such a phase originates

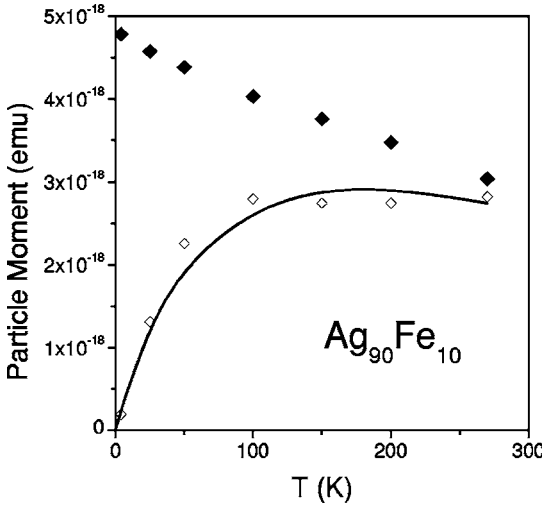

FIG. 2. Effective magnetic moment on Fe nanoparticles in $Ag_{90}Fe_{10}$ as a function of temperature (open symbols, experimental results; solid line: ISP model). Solid symbols: true magnetic moment as predicted by ISP model. Crossed symbols: results below T_B (marked by the dashed vertical line).

from weak, long-range interactions among isolated nanoparticles of a ferromagnetic metal in a nonmagnetic host. The ISP phase usually occurs at intermediate temperatures between a low-T blocked phase and a high-T superparamagnetic (SP) phase. Analysis of field-cooled and zero-field-cooled (FC-ZFC) curves[22] reveals that in $Ag_{100-x}Fe_x$ films with $x \leqslant 20$ the blocking temperature increases with x ($T_B = 28.5, 70, 160$ K for $x = 10, 14, 20$, respectively).

The ISP model allows one to obtain a correct estimate of the mean magnetic moment on nanoparticles and of their density. When interparticle interactions are no longer negligible, a standard fit of isothermal magnetization curves to a Langevin function (or a superposition of Langevin functions) results in systematically underestimating the particle moment;[21] in fact, the standard fitting procedure provides an *effective* magnetic moment, not the true one. The effective moment first increases linearly with absolute temperature, to eventually merge with the true magnetic moment at high T.[21,23] This behavior is observed in $Ag_{100-x}Fe_x$ films with $x \leqslant 20$ (see Fig. 2, open symbols, $x=10$). The curve contains the effective magnetic-moment values obtained by applying the ISP model at all temperatures. Of course, the ISP model cannot be applied below T_B: therefore, the points at $T=4$ K and $T=25$ K should be considered as merely indicative (they have been included in Fig. 2 as crossed symbols). In an ISP system, it is possible to perform a specific analysis, allowing one to estimate the true magnetic moment on particles and the number of particles per unit volume, N. Details of the procedure have been provided elsewhere.[21] The results of the ISP analysis performed in films with $x = 10, 14, 20$ are summarized in Table I. The interparticle distance d is equal to $1/N^{1/3}$; the nanoparticle diameter is obtained from the low-temperature value of the true magnetic moment μ using the saturation magnetization of bulk Fe. Incidentally, the diameter-to-distance ratio emerging from the ISP analysis (next to last column in Table I) takes values very close to the prediction based on simple geometrical arguments when it is assumed that all Fe atoms are included in spherical, equally spaced nanoparticles. In that case, the diameter-to-distance ratio is expected to be equal to

$$\frac{2r}{d} = \left(\frac{6x}{100\pi}\right)^{1/3}, \tag{1}$$

where x is the relative Fe concentration. The values obtained from Eq. (1) are shown in Table I (last column). The agreement again indicates that the ISP model correctly describes $Ag_{100-x}Fe_x$ films with $x \leqslant 20$. The present particle size estimates are in fairly good agreement with figures obtained on the same films by other methods. Neutron scattering measurements performed on films with $x = 10, 20$ give $2r = 1.4$ nm in both cases; fitting of magnetization curves through a lognormal distribution of particle sizes provides $2r = 1.2$ nm for $x = 10$ and $2r = 3.4$ nm for $x = 20$.[24]

The temperature behavior of the true magnetic moment[21] of $Ag_{90}Fe_{10}$ is reported in Fig. 2 (solid symbols). The solid line represents the model's prediction for the effective moment and is in good agreement with the experimental results (open symbols). A similar behavior is observed in films with $x=14$ and 20, although the ISP analysis is somewhat less satisfactory in the $x=20$ case, indicating that the upper limit of validity of the approach has been reached.

In fact, films with $x > 20$ exhibit a completely different magnetic behavior. The ZFC curve of $Ag_{74}Fe_{26}$ still exhibits a broad, shallow maximum, possibly indicating a blocking temperature of 238 K, while that of $Ag_{70}Fe_{30}$ no longer exhibits any distinguishable maximum between 2 and 300 K.[22] Magnetization data on $Ag_{100-x}Fe_x$ films with $x > 20$ were published elsewhere.[25] In those films, a large magnetization step occurring at low fields is followed by a much slower approach to saturation. This behavior is distinctive of a frustrated ferromagnetic phase, which has been observed in other systems, such as chemically homogeneous $Au_{70}Fe_{30}$ (at room temperature) and $Au_{80}Fe_{20}$ (at low temperatures).[14]

TABLE I. Summary of ISP analysis in films with $x \leqslant 20$. N: number of Fe particles per unit volume. d: mean interparticle distance. $2r$: mean diameter of Fe particles. $(2r/d)_{expt}$ and $(2r/d)_{theor}$: actual and ideal diameter-to-distance ratio.

Alloy	N [cm^{-3}]	d [nm]	$2r$ [nm]	$(2r/d)_{expt}$	$(2r/d)_{theor}$
$Ag_{90}Fe_{10}$	356×10^{19}	3.0	1.8	0.60	0.58
$Ag_{86}Fe_{14}$	3.14×10^{19}	3.2	2.0	0.64	0.65
$Ag_{80}Fe_{20}$	116×10^{19}	4.5	3.2	0.71	0.75

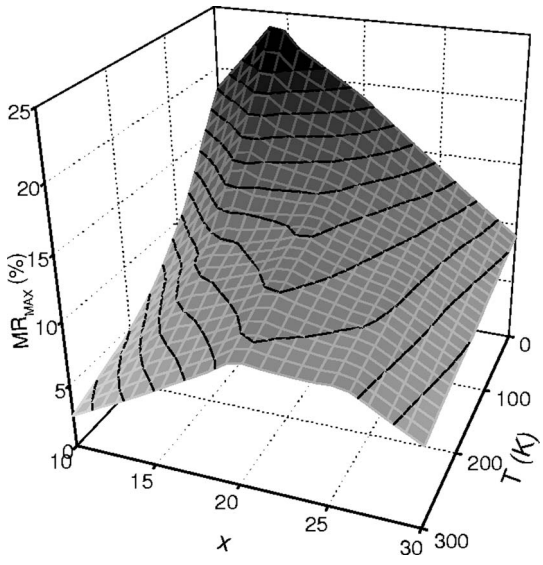

FIG. 3. Maximum magnetoresistance in $Ag_{100-x}Fe_x$ films as a function of measurement temperature and Fe content.

IV. RESULTS: MAGNETORESISTANCE MEASUREMENTS

Measurements of MR_{max} as a function of x and T (Ref. 26) provide a complete set of data which are exploited to build a surface in a three-dimensional (3D) space (see Fig. 3). Contours of equal MR_{max} levels are drawn in black. At all temperatures, MR_{max} attains its maximum value at an intermediate Fe concentration; at very low temperatures, the maximum is steeper and centered around $x=15$, while at $T=270$ K it is much broader and occurs around $x=21$—i.e., close to the percolation limit x_p for the $Ag_{100-x}Fe_x$ system ($x_p \simeq 20$).[27] MR_{max} generally increases with decreasing temperature. The MR of $Ag_{90}Fe_{10}$ (squares) and $Ag_{70}Fe_{30}$ (circles) is reported as a function of applied field in Fig. 4(a); open symbols refer to $T=270$ K, solid symbols to $T=4$ K. The same data are plotted as functions of reduced magnetization $m=M/M_S$ in Fig. 4(b). In the film with $x=10$, a nearly parabolic behavior is found at high temperatures; in films with $x \geqslant 20$, severe flattening of the MR(m) curves is systematically observed at low m. This is shown in Fig. 4(c), where the extremal cases ($Ag_{90}Fe_{10}$, $T=270$ K and $Ag_{70}Fe_{30}$, $T=2$ K) are plotted as functions of the square of reduced magnetization. Parabolic or nearly parabolic behavior of MR(m) is a distinctive feature of the isotropic giant magnetoresistance of nanogranular systems with almost uncorrelated moments.[5] On the other hand, severe flattening of the MR(m) curves has been found in frustrated ferromagnets well below the paramagnetic transition temperature.[14] In that case, MR(m) has a much squared shape with almost rectilinear edges, as in Figs. 4(b) and 4(c) ($x=30$). This behavior appears in ferromagnetic systems characterized by ultrashort ferromagnetic exchange length, typically extending from a few nanometers to some hundreds of nanometers.[17]

The MR(H) curves [Fig. 4(a)] did not display any evidence of magnetoresistance effects other than the negative MR ascribed here to GMR or to proximity magnetoresistance (PMR).[14] In particular, no evidence of anisotropic magnetoresistance (AMR) from ferromagneticlike regions was observed in films with x above the percolation threshold. Admittedly, the measurements on our sample's films were performed in the longitudinal configuration only, as previously remarked, but the simultaneous presence of GMR and AMR is often detectable not only from the different behavior in longitudinal or transverse configuration, but also on the basis of their behavior as a function of H (see, for instance, Ref. 28). On the other hand, all frustrated magnets discussed in Ref. 17 were submitted to magnetoresistance measurements in both the longitudinal and transverse configurations, and no significant anisotropic magnetoresistance was detected in that case.

V. ANALYSIS OF THE MAGNETIC CORRELATION

A. Magnetic correlation ratio and magnetic correlation length

According to a recent model,[17] the shape of the MR(m) curves is unequivocally related to the ratio between a radius of magnetic correlation, $R_m(H,T)$, and the average mean free path λ (at zero applied field) of electrons scattered by magnetization discontinuities. These typically occur either at the magnetic/nonmagnetic interfaces in nanoparticle systems or at the edges of correlation regions in frustrated ferromagnets. The magnetic correlation ratio $R_m(H,T)/\lambda(T)$ enters the following expression:[17]

$$R^* - R = \alpha[(\langle u^2\rangle - m^2)e^{(-\lambda/R_m)} + (1-\langle u^2\rangle)e^{(-2\lambda/R_m)}], \quad (2)$$

where R is the measured electrical resistance, $u=\cos\theta$ is the cosine of the angle between the local magnetization vector and the field axis, the reduced magnetization m is the thermal average $\langle u\rangle$, $\langle u^2\rangle$ can be expressed in terms of m by spherical random walk arguments as[17]

$$\langle u^2\rangle = \frac{1}{3} + \frac{2}{3}m^3, \quad (3)$$

α is a constant, and R^* is the parabolic curve which interpolates the high-field experimental resistance versus magnetization data [see Fig. 4(c)]:

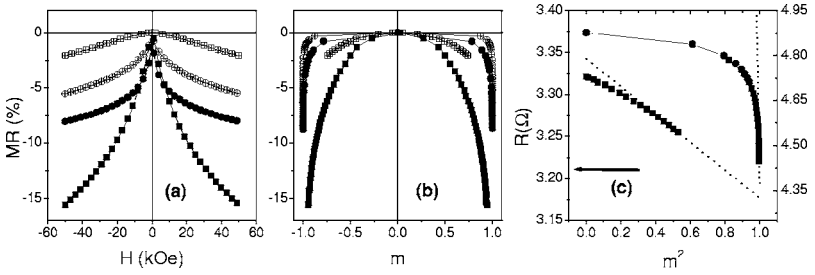

FIG. 4. (a) Magnetoresistance in $Ag_{90}Fe_{10}$ (squares) and $Ag_{70}Fe_{30}$ (circles) as a function of applied magnetic field. Solid symbols: 2 K. Open symbols: 270 K. (b) Same data as in (a), plotted as functions of reduced magnetization m. (c) Magnetoresistance in $Ag_{90}Fe_{10}$ at $T=270$ K (squares) and in $Ag_{70}Fe_{30}$ at $T=4$ K (circles) as a function of m^2. Straight lines indicate parabolic behavior at high fields.

$$R^* = R_0 - \beta m^2, \tag{4}$$

R_0 and β being fitting constants. Equation (2) allows one to accurately determine the magnetic correlation ratio as a function of temperature and magnetic field.[17] The absolute correlation radius can be obtained from the value of λ (estimated through the Drude formula) and the experimental temperature variation of the sample resistance.

Actually, Eq. (2) holds in bulk frustrated magnets.[17] In the following, however, this equation will be applied to both frustrated magnets ($x > 20$) and granular systems ($x \leqslant 20$). In principle, Eq. (2) should be substituted in granular systems by a more complex formula involving *two* correlation ranges (R_θ, R_ϕ) instead of one.[15] On the other hand, it was experimentally shown that R_θ and R_ϕ are linearly correlated, albeit not equal, in all studied granular alloys.[15,29] As a consequence, Eq. (2) will be used here on granular alloys also, with the proviso that R_m be considered as a suitable average of R_θ and R_ϕ.

All considered films, independent of the Fe concentration, exhibit a structural inhomogeneity deriving from the preparation technique and the immiscibility of elements. While at low Fe concentration our films are both structurally and magnetically inhomogeneous, films with $x > 20$ exhibit a higher magnetic homogeneity, such that a single region where the moments are correlated typically encompasses many Fe particles, both isolated and coalesced (or the exchange correlation length is greater than the mean interparticle distance). Therefore, the short-distance structural inhomogeneity is significantly smeared out by long-ranged magnetic correlation. For this reason, it is believed that the approach introduced in Ref. 17, although originally developed for *homogeneous* solid solutions, can still be applied with good reliability to the present films with $x > 20$.

The magnetic correlation radius defines a volume centered at any magnetic site, where all magnetic moments are correlated with the central one. Correlation does not mean parallelism;[17] it merely corresponds, in the ideal case, to a coherent response of the whole set of correlated moments to any external disturbance, of either magnetic or thermal origin. Therefore, both spatial and temporal aspects are present in our definition of magnetic correlation. The coherent response of correlated moments to a sudden magnetic field change can be viewed as a temporal correlation, while the correlation length defines the correlation in space. Evaluating the actual degree of parallelism (ferromagneticlike alignment) of magnetic moments in a correlation region is a different matter, which will be briefly discussed in the following (see Sec. V B).

Well below the percolation limit, magnetic nanoparticles are in principle separated and interacting through noncontact interactions; in this case, the following geometrical model can be adopted (see Fig. 5): the nanoparticles are considered as identical spherules, equal in size and forming a regular cubic array of pitch d. Particle size and interparticle distance are those obtained from the ISP analysis of the previous section. The correlation volume corresponds to a cube of edge $L_{corr} = 2R_m$. The ratio L_{corr}/d plays a central role, because the condition $L_{corr}/d \leqslant 1$ means the absence of interparticle correlation (pure SP phase), while values larger than unity are associated with the ISP phase. The number of correlated nanoparticles, n_{corr}, is given by $(L_{corr}/d)^3$, because the number of particles per unit volume is $1/d^3$. In a real simple cubic lattice, the quantity n_{corr} would increase by discrete steps, in particular when L_{corr} is not much larger than d; in our model, however, this constraint can be removed, because d and L_{corr} are average values in a material actually containing a spectrum of interparticle distances and local correlation lengths. As a consequence, n_{corr} is assumed to change in a continuous way.

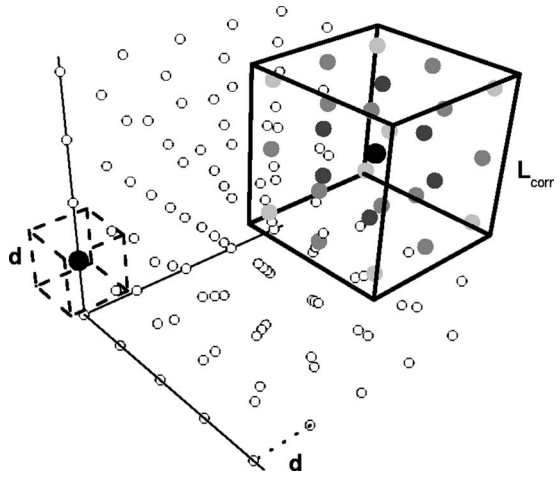

FIG. 5. Simplified model of nanogranular $Ag_{100-x}Fe_x$ ($x < 20$). d: mean interparticle distance. L_{corr}: correlation length. Open circles: magnetic nanoparticles. Different levels of gray indicate the fading magnetic correlation to the central moment (large black dot) inside the cubic correlation volume.

Apparently, this scheme cannot be applied to systems with Fe concentrations above the percolation limit ($x > 20$); in such a case, the correlation volume can still be assumed to be a cube of edge $L_{corr} = 2R_m$; however, the ratio L_{corr}/d is no longer of use, because the particles lose their individuality (many of them touch each other, creating physical aggregates governed by contact interactions).

The temperature behavior of $L_{corr} \equiv L_{corr}(H=0)$ is reported in Fig. 6(a) for all studied alloys. Note the vertical logarithmic scale. Horizontal lines mark the d values for $x = 10, 14, 20$. It can be observed that (a) all L_{corr} values of granular films with $x \leqslant 20$ are larger than the corresponding d distances; (b) in these films, the separation between L_{corr} and d decreases monotonically with increasing temperature, while L_{corr} increases with increasing x at any temperature; (c) in $Ag_{90}Fe_{10}$, L_{corr} closely approaches d_{10} at high temperatures; this film is therefore the only one actually on the way of becoming a pure SP system, as confirmed by the nearly parabolic shape of the MR(m) curve.

On the other hand, films with $x > 20$ are characterized by much larger correlation lengths, clearly indicating a magnetic arrangement typical of a frustrated ferromagnet. In these films, L_{corr} provides a figure of the ferromagnetic exchange length. In the case of the film with $x = 26$, L_{corr} decreases at high temperatures; this is likely to be related to the proximity of the alloy's Curie temperature T_C, as previously observed

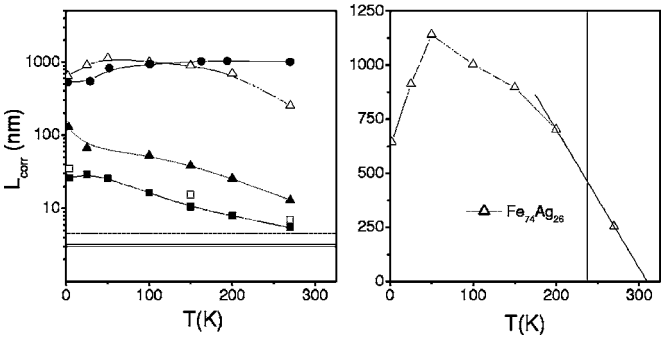

FIG. 6. (a) Magnetic correlation length as a function of temperature in $Ag_{100-x}Fe_x$-cosputtered films (■, $x=10$; □, $x=14$; ▲, $x=20$; △, $x=26$; ●, $x=30$). Mean interparticle distances for $x=10,14,20$ are indicated by horizontal lines (solid line, $d_{10}=3.0$ nm and $d_{14}=3.2$ nm; dashed line, $d_{20}=4.5$ nm). (b) Magnetic correlation length as a function of temperature in $Ag_{74}Fe_{26}$ (linear scale for the vertical axis). Solid line: high-temperature extrapolation to $L_{corr}=0$. Dotted vertical line: T_B.

in similar frustrated ferromagnets.[30] In fact, a vanishingly small correlation length is expected above T_C.[31] The temperature variation of L_{corr} in $Ag_{74}Fe_{26}$ is reported in Fig. 6(b) on a linear scale. The paramagnetic Curie temperature of this film can be estimated through linear extrapolation of L_{corr} to zero (solid line); the resulting T_C is equal to 310 K. The Curie temperature of the film with $x=30$ must be significantly higher, as suggested by the nearly constant behavior of L_{corr} at high T.

Finally, the $Ag_{80}Fe_{20}$ film exhibits intermixed features between granular systems and frustrated ferromagnets.

In conclusion, the magnetic correlation lengths determined using Eq. (2) appear as a self-consistent set of data, supporting the idea of a progressive increase of magnetic correlation and complexity with increasing Fe concentration.

B. Initial magnetic susceptibility in granular films

Let us consider $Ag_{100-x}Fe_x$ films with lower Fe content ($x=10,14$). Our analysis indicates that the magnetic ordering units are not single moments on individual particles, but magnetic aggregates composed of many particles. Such a picture only holds at low to moderate external fields, because large fields act to degrade the correlation volumes: in fact, at very high fields, the correlation among moments disappears.[15,17] Measuring the initial magnetic susceptibility of these films is a good way to test the validity of the picture. In a standard SP system, this quantity is expected to take the value

$$\chi_0^{SP} = \frac{N\mu^2}{3kT}, \tag{5}$$

where $N=1/d^3$ is the number of particles per unit volume and $\mu=\mu(T)$ is the average true magnetic moment (Fig. 2). The saturation magnetization is $M_S=N\mu$, so that the reduced susceptibility is simply

$$\tilde{\chi}_0^{SP} = \frac{\mu}{3kT}. \tag{6}$$

The experimental $\tilde{\chi}_0$ vs T curve for $x=10,14$ is in excellent agreement with this prediction well above the blocking temperature, as expected. The deviation between the experimental $\tilde{\chi}_0(T)$ curve and Eq. (6) increases with decreasing T below about $3T_B$, indicating that the system is gradually losing the pure SP behavior. The reduced initial susceptibility $\tilde{\chi}_0$ of $Ag_{100-x}Fe_x$ films has been measured by taking the field derivative of isothermal $m(H)$ curves and found to increase with increasing magnetic correlation length. The results are plotted in Figs. 7(a) and 7(b) as functions of the square of the ratio L_{corr}/d. A nearly linear behavior is observed for each alloy (solid symbols). Quite interestingly, linear extrapolation of experimental data to $L_{corr}/d=1$ gives in both cases a value practically coincident with the SP prediction at $T=270$ K [Eq. (5), large crossed symbols in Figs. 7(a) and 7(b)]. This is precisely what is expected when the correlation volume is so small that it contains only the central moment: at high temperatures, both granular films must approach the SP behavior, as already remarked.

The increase of $\tilde{\chi}_0$ with L_{corr} can be explained considering that the ordering units are aggregates of moments. Let μ_{corr} be the effective moment of an aggregate containing n_{corr} moments. Our estimates for L_{corr} indicate that in $Ag_{90}Fe_{10}$, n_{corr} is as small as ≈ 10 above 200 K, reaching the value of ≈ 1000 at very low temperatures. The number of aggregates per unit volume is $N_a=N/n_{corr}$. At low applied fields, each aggregate responds as a whole; the reduced susceptibility is therefore

$$\tilde{\chi}_0 = \frac{1}{M_S}\frac{N_a\mu_{corr}^2}{3kT} = \frac{N_a}{N}\frac{\mu_{corr}^2}{\mu}\frac{1}{3kT}. \tag{7}$$

Recalling that $n_{corr}=(L_{corr}/d)^3$, the initial reduced susceptibility becomes

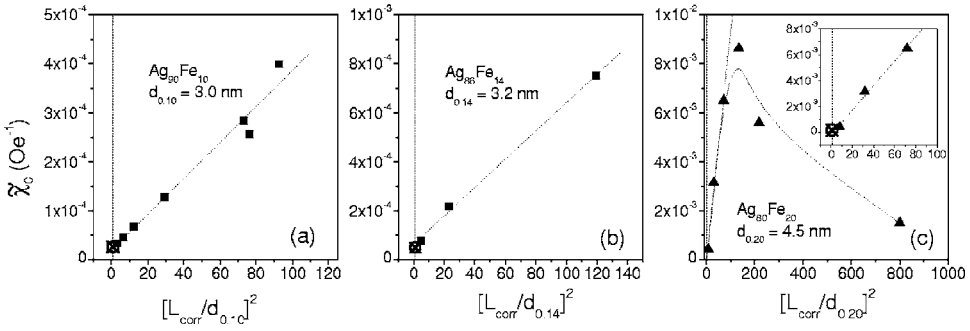

FIG. 7. Reduced initial susceptibility as a function of $(L_{corr}/d)^2$ for $x=10,14,20$. Inset in (c): expanded low $(L_{corr}/d)^2$ region. Thick crossed symbols: predicted susceptibility of the superparamagnetic phase ($L_{corr}/d=1$) at $T=270$ K.

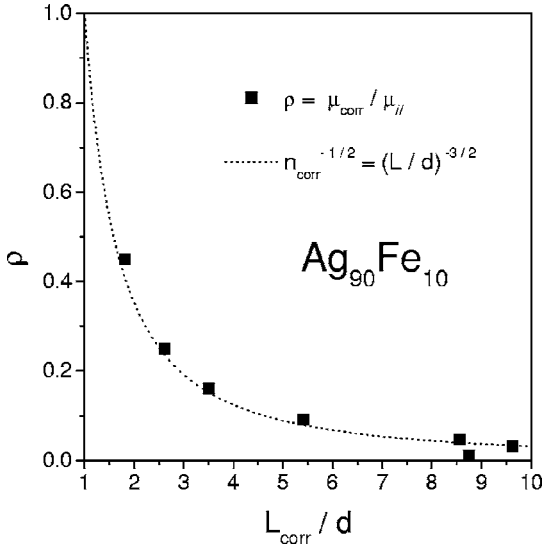

FIG. 8. Ratio ϱ between actual and maximum magnetic moments of a correlation volume as a function of L_{corr}/d in $Ag_{90}Fe_{10}$. Dotted line: $n_{corr}^{-1/2}$.

$$\tilde{\chi}_0 = \frac{\mu_{corr}^2}{\mu}\frac{1}{3kT}\frac{1}{(L_{corr}/d)^3}. \tag{8}$$

Now, the effective moment of an aggregate cannot be larger than the quantity $\mu_{\|}=n_{corr}\mu \equiv (L_{corr}/d)^3\mu$, corresponding to the case of perfectly aligned moments. In this limit, the reduced initial susceptibility becomes

$$\tilde{\chi}_{0\|} = \left(\frac{L_{corr}}{d}\right)^3 \frac{\mu}{3kT} \equiv \left(\frac{L_{corr}}{d}\right)^3 \tilde{\chi}_0^{SP}; \tag{9}$$

i.e., it is predicted to increase with increasing L_{corr}/d, but according to a *cubic*, not a nearly quadratic, dependence law as instead observed. Such a discrepancy is related to imperfect alignment of magnetic moments in the correlation volume. In fact, the quantity μ_{corr} can be directly obtained from experimental data through Eq. (8) as

$$\mu_{corr} = \left[3kT\mu(T)\tilde{\chi}_0\left(\frac{L_{corr}}{d}\right)^3\right]^{1/2}. \tag{10}$$

Let us consider the ratio $\varrho=\mu_{corr}/\mu_{\|}$, plotted as a function of L_{corr}/d in Fig. 8 for $Ag_{90}Fe_{10}$ (similar results are obtained for $x=14$). This quantity can be considered as a measure of the average degree of alignment of individual magnetic moments in any correlation volume. The case $\varrho=1$ corresponds to perfect parallel alignment; $\varrho=0$ indicates random directions of individual moments within the aggregate (actually, it could correspond to perfect antiparallel alignment of moments also, but the possibility is disregarded here); in fact, net antiferromagneticlike correlations would *increase* the zero-field GMR with respect to the ideal case of uncorrelated particles, which is not observed in these films [see Fig. 4(c)]. As a matter of fact, *dominant* antiferromagnetic interactions are seldom found in similar systems.[32,33] In the literature, the presence of antiferromagnetic interactions in granular systems is often implied by the observation of a negative intercept of the $1/\chi_0(T)$ curve;[34] it should be noted, however, that the same feature is predicted by the ISP model without requiring that the dominant interactions among moments be strictly antiferromagnetic in nature.

The behavior reported in Fig. 8 indicates that individual moments are indeed more ferromagnetically aligned inside small correlation volumes than inside larger ones. However, perfect ferromagneticlike alignment is never attained, even in the smallest observed correlation region ($L_{corr}/d\simeq 2$). Only a partial alignment is observed, an indication of competing interactions among magnetic moments. However, these act to cancel out each other only in the limit of large correlation regions, so that the spread of magnetic moment directions increases with decreasing temperature. Such a behavior could prefigure the onset of low-temperature static disorder of magnetic moments in the granular material, which undergo random freezing below the blocking temperature.

The observed behavior of ϱ is fully compatible with the function $n_{corr}^{-1/2}$ (dotted line in Fig. 8). This is a remarkable result, because an inverse dependence on the square root of correlated magnetic entities is expected to be found in disordered systems on the basis of random walk considerations.[35,36] In amorphous ferromagnetic alloys, for instance, the effective anisotropy equals the local anisotropy divided by the square root of the number of grains in the volume defined by the exchange length.[35] A similar scheme was used by Denardin *et al.*[37] to reconcile ZFC and FC curves and transmission electron microscopy (TEM) data taken in the insulating nanogranular material $Co_x(SiO_2)_{1-x}$. The present result strongly suggests a similar mechanism acting in granular $Ag_{100-x}Fe_x$ films, the correlation length playing a role equivalent to the exchange length in amorphous ferromagnets.

Finally, let us remark that the $Ag_{80}Fe_{20}$ composition once again marks the onset of a different magnetic behavior. This is particularly evident in Fig. 7(c): at low L_{corr}/d, a linear behavior of $\tilde{\chi}_0$ is still observed, and extrapolation to $L_{corr}/d=1$ still provides a value compatible with the SP prediction [crossed symbol in the inset of Fig. 7(c)]; at higher L_{corr}/d, however, the initial linear trend is lost and the measured initial susceptibility drops. Recalling that a high L_{corr}/d is found at low temperatures, this result means that magnetic interactions among closer particles act to set up a blocked state of low initial susceptibility below about 150 K. At higher temperatures, the film can be approximately considered as an interacting superparamagnet. This is in good agreement with the blocking temperature $T_B\approx 160$ K obtained by FC and ZFC curves.[22]

C. High-field magnetic susceptibility and magnetic correlation length

The magnetic susceptibility at high fields ($H=50$ kOe) has been measured in all $Ag_{100-x}Fe_x$ films. The temperature behavior of the reduced susceptibility $\tilde{\chi}_{50\ \mathrm{kOe}}$ of the sample with $x=10$ is reported in Fig. 9 (solid symbols) along with the prediction of the standard SP model:

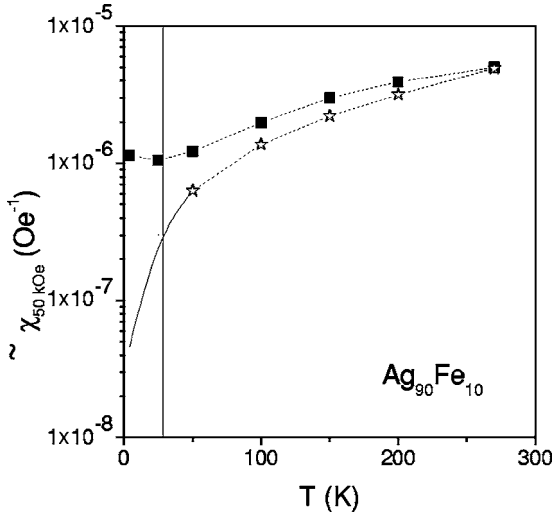

FIG. 9. Reduced susceptibility at $H=50$ kOe in $Ag_{90}Fe_{10}$ as a function of temperature. Solid squares: experiment. Open symbols: SP model. T_B marked by the solid vertical line.

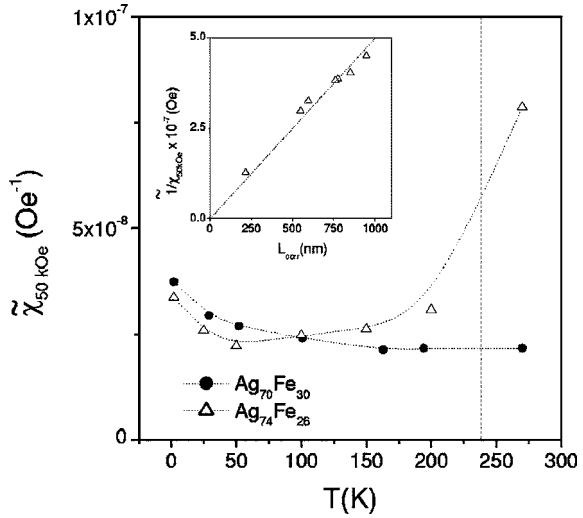

FIG. 10. Reduced susceptibility at $H=50$ kOe in $Ag_{70}Fe_{30}$ and $Ag_{74}Fe_{26}$ as a function of temperature. Dashed vertical line: presumed blocking temperature for $Ag_{74}Fe_{26}$. Inset: inverse of reduced susceptibility of $Ag_{74}Fe_{26}$ as a function of L_{corr}.

$$\tilde{\chi}_{50\ \mathrm{kOe}} = \frac{kT}{\mu H^2|_{H=50\ \mathrm{kOe}}} \tag{11}$$

(open symbols). Of course, the SP model loses validity below the blocking temperature (i.e., 28.5 K in this case); the curve at very low temperatures is still shown in the figure, but as a solid line. At $T=270$ K, the measured susceptibility is almost coincident with the SP prediction, as expected; this is another check of the validity of the present analysis. Below 270 K, the measured susceptibility is higher than predicted by the SP model, the distance between curves gradually increasing with reducing T. This means that the film has a less saturating behavior than a standard superparamagnet, in good agreement with the presence of effective ordering units larger than a single moment even at high fields. In other words, the correlation length L_{corr}, even if reduced with respect to the zero-field value, is still larger than d.

On the other hand, films with $x>20$ again exhibit a different behavior, as shown in Fig. 10. In $Ag_{70}Fe_{30}$, $\tilde{\chi}_{50\ \mathrm{kOe}}$ stays constant on cooling between 270 and 150 K, and displays a significant increase when the temperature is further lowered. In $Ag_{74}Fe_{26}$, a similar low-temperature trend is observed; however, the main feature here is the strong increase at high temperatures. The common low-temperature rise of $\tilde{\chi}_{50\ \mathrm{kOe}}$ indicates that a long-ranged ferromagnetic order does not exist in these films, as already observed in some $Au_{100-x}Fe_x$ alloys;[30] this is in agreement with the picture of $Ag_{100-x}Fe_x$ films with $x>20$ as frustrated ferromagnets. The high-temperature increase observed in $Ag_{74}Fe_{26}$ is a feature usually associated with a paramagnetic transition being approached from below. A similar effect has already been observed in $Au_{80}Fe_{20}$.[30] This result is in agreement with the reduction of the magnetic correlation length taking place in $Ag_{74}Fe_{26}$ in the same temperature region [see Fig. 6(b)]. The inset in Fig. 10 shows that the high-field reduced susceptibility of $Ag_{74}Fe_{26}$ is inversely proportional to the magnetic correlation length L_{corr}.

D. Functional dependence of L_{corr} on the magnetic field

Another interesting point is the stability of magnetic correlation regions under the effect of a magnetic field. As previously remarked, the magnetic correlation length is a function of H, becoming vanishingly small at sufficiently high fields. In frustrated ferromagnets, the correlation ratio R_m/λ was found to monotonically decrease with H. No simple dependence law is observed;[17,38] however, after a very fast decay at low H, at high fields $R_m(H)/\lambda$ asymptotically behaves as a single exponential of the form $e^{-H/H_{corr}}$. The correlation field H_{corr} is such that when $H \gg H_{corr}$, the width of the coherence regions is significantly less than the electron mean free path λ.

In $Ag_{100-x}Fe_x$ films with $x>20$, the magnetic correlation length follows a quite similar behavior—i.e., a fast initial decay ending up with an asymptotic exponential law. On the other hand, films with low Fe content exhibit at low temperatures a perfect single-exponential behavior starting from $H=0$, as shown in Fig. 11 for $Ag_{90}Fe_{10}$. Fitting these data to the function

$$L_{corr}(H) = L_{corr}(0)e^{-H/H_{corr}} \tag{12}$$

allows one to determine the value of H_{corr} (≈ 18 kOe in the considered case). At higher temperatures, however, the initial decay is markedly less steep than an exponential. At high fields, all $L_{corr}(H)$ curves merge, indicating that the high-field L_{corr} data points asymptotically follow the same exponential law with the same H_{corr}. This effect can be described in the following way: both T and H independently act to destroy the magnetic correlation volumes; at low temperatures, where $L_{corr}(0)$ is a maximum and does not significantly vary with T, the magnetic field immediately acts to reduce L_{corr}. At higher temperatures, the starting correlation volumes are much smaller, because $L_{corr}(0)$ has been lowered by thermal disorder. The plots of Fig. 11 suggest that initially smaller correlation volumes are more resistant to the action of a mag-

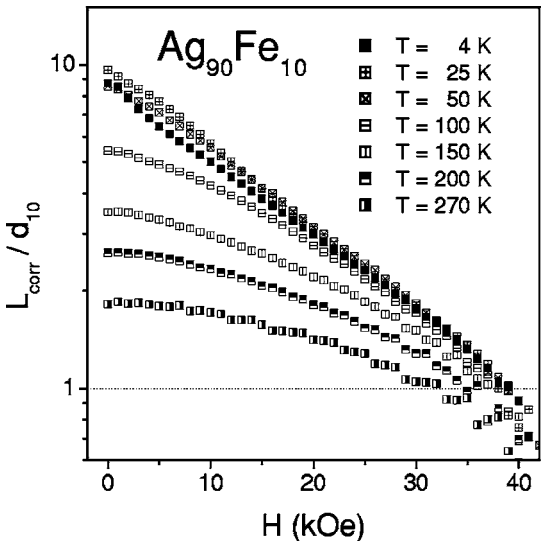

FIG. 11. Behavior of L_{corr}/d as a function of magnetic field in $Ag_{90}Fe_{10}$ at different temperatures.

netic field than initially larger ones. In order to further investigate this point, we have determined, for all compositions and at all temperatures, the value of $H_{1/3}$ corresponding to a reduction of L_{corr} to one-third of the starting value, independently of the actual variation of L_{corr} with H. This quantity is plotted in Fig. 12 as a function of the zero-field correlation volume $V_{corr}(0)=L_{corr}^3$. Quite remarkably, the data taken on all examined samples approximately fall on one curve; data sets from different samples define different portions of this master curve, with a progressive shift and no significant gap within them. This result indicates that a single functional law relates the initial correlation volume size to its stability under a magnetic field, quite independently of the alloy composition. However, no simple power law fits the actual behavior of $H_{1/3}$ with correlation volume. Saturating trends are observed at low and high volumes; intermediate data points

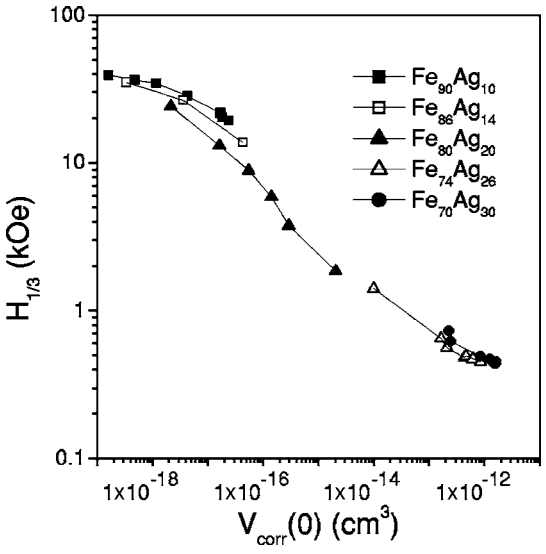

FIG. 12. Dependence of $H_{1/3}$ on zero-field correlation volume in all studied films (see text).

roughly follow a power law with an exponent between $-1/2$ and $-1/3$. Random-walk arguments would suggest a dependence of the type $n_{corr}^{-1/2} \sim V_{corr}(0)^{-1/2}$ throughout. Apparently, a more complex functional law is followed.

VI. CONCLUDING REMARKS

$Ag_{100-x}Fe_x$-cosputtered films are an example of granular bimetallic alloys with a variable degree of correlation among magnetic moments. Magnetic correlation steadily increases with Fe concentration, giving rise to different equilibrium magnetic configurations and to a different magnetization process. A detailed picture of the increasing magnetic complexity has been obtained from simultaneous measurements of isothermal magnetization and magnetoresistance, exploiting the intrinsic sensitivity of MR to the degree of correlation of moments on the scale of the electron mean free path.

The proposed picture succeeds in representing the magnetic behavior of an entire family of granular alloys through simple unifying concepts. On the other hand, it neglects the effect of local variations in the magnetic arrangement related to a number of specific causes, such as sample inhomogeneity, surface roughness, variation of magnetic properties with film thickness, substrate effects, and oxidation. In addition, it takes into account average values of magnetic moments and interparticle distances, rather than their actual distributions. Despite these limits, the picture has an inner coherence and it provides a set of consistent results. They are summarized as follows.

(i) Magnetic correlation generally increases with Fe concentration and on reducing temperature, so that a variety of magnetic states, from simple to complex, emerge in the considered range of x values. The simplest state corresponds to the pure superparamagnetic phase, which can be viewed as a high-temperature limit in $Ag_{90}Fe_{10}$ and $Ag_{86}Fe_{14}$. In fact, pure SP behavior has never been directly observed in the present measurements. The magnetic interaction among physically separated moments can never be totally neglected; when it is weak enough, the ISP phase emerges, as in films with x below the percolation limit. Magnetic aggregates composed of all moments inside a correlation volume appear there as the ordering units. In ISP-type films, Fe nanoparticles still retain their physical individuality (they do not touch each other) but they progressively lose their *magnetic* individuality. On the other hand, above the percolation limit, Fe particles lose their physical individuality as well. In this case, competing interactions (contact and noncontact) among magnetic moments result in a frustrated ferromagnetic state, characterized by a paramagnetic Curie temperature T_C and a finite exchange correlation length, essentially coincident with L_{corr}. The examined frustrated ferromagnets ($x=26,30$) remain below the Curie temperature; in $Ag_{74}Fe_{26}$, T_C is not much above the upper limit of the investigated temperature interval, while in $Ag_{70}Fe_{30}$ the paramagnetic transition is displaced towards higher temperatures.

(ii) In ISP-type films, the magnetic moments within a correlation volume are generally not aligned; the degree of alignment scales with the inverse of the square root of the number of correlated moments, in agreement with random-

walk arguments and in analogy with the prediction of the random-anisotropy model in other disordered magnetic systems.

(iii) The threshold for the onset of frustrated ferromagnetism is slightly above the percolation limit $x_p=20$. The film with $x=20$ still retains the features of the ISP phase, but with a very extended low-temperature blocked state. Therefore, it can still be described as a magnetically granular system; no sharp transition to a frustrated ferromagnetic phase is observed in it.

(iv) In all films, the correlation volumes have greater stability against an external magnetic field when they are smaller; the largest stability is exhibited by aggregates of a few tenths of particle moments, such as in $Ag_{90}Fe_{10}$ at high temperatures. These small volumes, bearing a nonzero total magnetic moment, can be easily aligned as a whole by a weak external field; the field intensity needed to destroy the inner magnetic correlation is, however, much higher ($\approx$40 kOe).

A final comment is devoted to possible alternative pictures of the same experimental data set. In this paper, flattening of MR(m) curves away from the ideal parabolic behavior has been considered as the hallmark of increasingly correlated magnetic systems, from an interacting superparamagnet to a frustrated magnet. As a matter of fact, the geometrical model proposed in this paper uses *average* values of geometrical and structural parameters, such as particle size and interparticle distance. On the other hand, in any granular system, a distribution of particle size (and interparticle distance) is generally expected.[37] Therefore, one should consider whether the magnetoresistance curves and their flattening could be explained by invoking an alternative explanation based more upon the presence of particles of different size rather than on magnetic correlations among them. In fact, alternative explanations of the functional dependence of the GMR on either magnetization or magnetic field based on the size distribution of the magnetic granules can be found in the literature.[39,40] Let us briefly discuss two possible scenarios: namely, (a) a narrow particle-size distribution, as often observed in nanogranular materials,[37,41] and (b) a bimodal distribution, with large ferromagnetic grains intermixed with much smaller SP particles. Let us neglect interparticle interactions. In the first case, the system generally consists of a blocked and a superparamagnetic fraction, with a different magnetic response. In principle, the shape of the MR(m) curve could be explained by such a picture, as proposed, for instance, in Ref. 41, where the flattening of the magnetoresistance curve was explained using the distribution of magnetic moments obtained from magnetization data (at room temperature only). However, this procedure may be misleading, because the true particle size distribution (i.e., one which is obtained by direct observation, such as TEM) has been shown to be systematically different from that obtained on the basis of magnetization measurements.[42] Obviously, the MR curve should reflect the true distribution of particle size, not the one obtained from magnetization curves, which can be significantly affected by interparticle interaction.[43] In conclusion, a conclusive proof of the adequacy of this alternative approach is still lacking.

In the second case, one would expect entirely different magnetization processes involving large grains and small particles. The GMR would essentially arise from small particles alone; magnetization would be dominated by large grains. However, additional magnetoresistance effects arising from large grains should be observed, such as anisotropic magnetoresistance, or domain-wall magnetoresistance. However, no experimental evidence of such contributions was found in the films with high Fe content in the considered $Ag_{100-x}Fe_x$ family (or in the frustrated magnets studied in Ref. 17).

In the light of the above comments, we suggest that the particle size distribution is less important than the interparticle interaction in determining the shape of the MR(m) curve. It can be presumed that a complete theory should take into account both contributions; the proposed model has the advantage of providing a self-consistent, quantitative description of the observed effects on the basis of the simplest hypothesis (δ-like particle size distribution).

ACKNOWLEDGMENTS

This work has been partially supported by FIRB-MIUR/INFM Project RBNE017XSW: "Microsystems Based on New Magnetic Materials Structured on the Nanoscopic Scale."

[1] H. Sun, C. B. Murray, D. Weller, L. Folks, and A. Moser, Science **287**, 1989 (2000).
[2] S. Morup and E. Tronc, Phys. Rev. Lett. **72**, 3278 (1994).
[3] J. Garca-Otero, A. J. Garca-Bastida, and J. Rivas, J. Magn. Magn. Mater. **189**, 377 (1998); **66**, 2152 (1991).
[4] A. E. Berkowitz, J. R. Mitchell, M. J. Carey, A. P. Young, S. Zhang, F. E. Spada, F. T. Parker, A. Hütten, and G. Thomas, Phys. Rev. Lett. **68**, 3745 (1992).
[5] J. Q. Xiao, J. S. Jiang, and C. L. Chien, Phys. Rev. Lett. **68**, 3749 (1992).
[6] M. N. Baibich, J. M. Broto, A. Fert, F. Nguyen Van Dau, F. Petroff, P. Etienne, G. Creuzet, A. Friederich, and J. Chazelas, Phys. Rev. Lett. **61**, 2472 (1988).
[7] S. S. P. Parkin, R. Bhadra, and K. P. Roche, Phys. Rev. Lett. **66**, 2152 (1991).
[8] J. R. Childress and C. L. Chien, Phys. Rev. B **43**, 8089 (1991).
[9] J. Wecker, R. von Helmolt, L. Schultz, and K. Samwer, Appl. Phys. Lett. **62**, 1985 (1993).
[10] G. Xiao, J. Q. Wang, and P. Xiong, Appl. Phys. Lett. **62**, 420 (1993).
[11] A. Lopez, F. J. Lazaro, M. Artigas, and A. Larrea, Phys. Rev. B **66**, 174413 (2002).
[12] J. A. De Toro, J. P. Andres, J. A. Gonzalez, J. P. Goff, A. J. Barbero, and J. M. Riveiro, Phys. Rev. B **70**, 224412 (2004).
[13] S. Zhang and P. M. Levy, J. Appl. Phys. **73**, 5315 (1993).
[14] P. Allia, M. Coisson, G. F. Durin, J. Moya, V. Selvaggini, P.

Tiberto, and F. Vinai, J. Appl. Phys. **91**, 5936 (2002).
[15] P. Allia, M. Knobel, P. Tiberto, and F. Vinai, Phys. Rev. B **52**, 15398 (1995).
[16] B. J. Hickey, M. A. Howson, S. O. Musa, and N. Wiser, Phys. Rev. B **51**, 667 (1995).
[17] P. Allia, M. Coisson, J. Moya, V. Selvaggini, P. Tiberto, and F. Vinai, Phys. Rev. B **67**, 174412 (2003).
[18] C. Yu, Y. Yang, Y. Zhou, S. Li, W. Lai, and Z. Wang, J. Appl. Phys. **76**, 6487 (1994).
[19] Y. Xu, K. Sumiyama, K. Wakoh, S. A. Makhlouf, and K. Suzuki, J. Appl. Phys. **76**, 2969 (1994).
[20] F. Spizzo, E. Angeli, D. Bisero, A. Da Re, F. Ronconi, and P. Vavassori, J. Magn. Magn. Mater. **272-276**, 1169 (2004).
[21] P. Allia, M. Coisson, P. Tiberto, F. Vinai, M. Knobel, M. A. Novak, and W. C. Nunes, Phys. Rev. B **64**, 144420 (2001).
[22] F. Spizzo (private communication).
[23] P. Allia, M. Coisson, P. Tiberto, and F. Vinai, J. Magn. Magn. Mater. **272-276**, E1189 (2004).
[24] F. Spizzo, E. Angeli, D. Bisero, A. Da Re, F. Ronconi, P. Vavassori, I. Bergenti, A. Deriu, and A. Hoell, J. Appl. Crystallogr. **36**, 826 (2003).
[25] P. Allia, M. Coisson, A. Da Re, F. Celegato, F. Spizzo, P. Tiberto, and F. Vinai, Phys. Status Solidi C **1**, 3406 (2004).
[26] P. Allia, M. Coisson, P. Tiberto, F. Vinai, D. Bisero, and F. Spizzo, IEEE Trans. Magn. **41**, 3412 (2005).
[27] J. Q. Wang and G. Xiao, Phys. Rev. B **49**, 3982 (1994).
[28] J. A. Mendes, V. S. Amaral, J. B. Sousa, L. Thomas, and B. Barbara, J. Appl. Phys. **81**, 5208 (1997).
[29] P. Allia, P. Tiberto, and F. Vinai, J. Appl. Phys. **81**, 4599 (1997).
[30] P. Allia, M. Coisson, J. Moya, V. Selvaggini, P. Tiberto, and F. Vinai, Phys. Status Solidi A **189**, 321 (2002).
[31] P. Allia, M. Coisson, V. Selvaggini, P. Tiberto, and F. Vinai, Phys. Rev. B **63**, 180404(R) (2001).
[32] D. Altbir, J. d'Albuquerque e Castro, and P. Vargas, Phys. Rev. B **54**, R6823 (1996).
[33] C. S. Martins and F. P. Missell, J. Appl. Phys. **89**, 7296 (2001).
[34] A. Gonzalez, P. Tiberto, A. Garcia-Escorial, D. Paramo, J. P. Sinnecker, P. Allia, and A. Hernando, J. Phys. IV **8**, Pr2-3433 (1998).
[35] G. Herzer, IEEE Trans. Magn. **26**, 1397 (1990).
[36] A. Hernando, M. Vazquez, T. Kulik, and C. Prados, Phys. Rev. B **51**, 3581 (1995).
[37] J. C. Denardin, A. L. Brandl, M. Knobel, P. Panissod, A. B. Pakhomov, H. Liu, and X. X. Zhang, Phys. Rev. B **65**, 064422 (2002).
[38] P. Allia, M. Coisson, V. Selvaggini, P. Tiberto, and F. Vinai, J. Magn. Magn. Mater. **262**, 39 (2003).
[39] J. Xu, B. J. Hickey, M. A. Howson, D. Greig, R. Cochrane, S. Mahon, C. Achilleos, and N. Wiser, Phys. Rev. B **56**, 14602 (1997).
[40] J. Balogh, L. F. Kiss, A. Halbritter, I. Kezsmarki, and G. Mihaly, Solid State Commun. **122**, 59 (2002).
[41] E. F. Ferrari, F. C. S. da Silva, and M. Knobel, Phys. Rev. B **56**, 6086 (1997).
[42] A. L. Brandl, L. M. Socolovsky, J. C. Denardin, and M. Knobel, J. Magn. Magn. Mater. **294**, 127 (2005).
[43] J. M. Vargas, W. C. Nunes, L. M. Socolovsky, M. Knobel, and D. Zanchet, Phys. Rev. B **72**, 184428 (2005).